J. W. Tierney

J. W. Eischen
Associate Professor,
Mem. ASME

Department of Mechanical and
Aerospace Engineering,
North Carolina State University,
Campus Box 7910,
Raleigh, NC 27695-7910

Residual Stress Analysis of Bimaterial Strips Under Multiple Thermal Loading

The residual stress distribution in bimaterial beams induced by multiple thermal loadings has been investigated. Three models for the nonlinear stress-strain material behavior were considered: bilinear elastic-plastic, power law elastic-plastic, and power law purely plastic. The equations governing equilibrium, compatibility of strain, and stress-strain for the bimaterial configuration make up a system of nonlinear algebraic equations which is solved numerically. The elastic-plastic power law model leads to stress discontinuity in the layers. The other two models have been verified with a finite element analysis. Several examples are included using materials common to the microelectronics industry.

Introduction

Significant temperature cycling is present in the manufacture of microelectronic devices as metallic layers are deposited onto a substrate to create a multilayered circuit or lead. The metal is heated to very high temperatures during chemical vaporization deposition. This is done for each layer, and the entire device is subjected to an annealing temperature after the top layer is deposited. A typical electronic device then has residual stress present through each layer after the manufacturing process is complete. A solution for this residual stress distribution is sought to be used as a design tool.

Timoshenko (1925) provided a solution for the resultant internal forces/moments and curvature induced in a bimaterial thermostat subjected to a single uniform temperature change. Both layers are treated as linear elastic. The method consists of enforcing zero resultant force and moment on the composite strip, and displacement compatibility. The problem was specialized to a thin film layer on a thick substrate by Suhir (1988), still assuming linear elastic materials. The analytical solution for the bimaterial configuration was extended by Cifuentes (1991) by allowing one of the layers to exhibit an elastic perfectly plastic stress-strain response. Eischen and Reagan (1993) further extended the work to include strain hardening and used a bilinear elastic plastic model for both layers. A more general power law stress-strain response was then included by Eischen and Reagan (1995). In all these cases, an analytical solution is obtained for the stress distribution due to a single uniform temperature load. Because electronic devices are subjected to repeated temperature cycles during manufacture and operation it is necessary to extend the previous work by allowing for the possibility of stress reversal and reverse yielding.

The present work is an extension of Eischen and Reagan (1993), where multiple piecewise constant thermal loads are allowed to act on the bimaterial strip. Both a bilinear and power law response model are treated, and an isotropic hardening model is assumed. A system of nonlinear algebraic equations is developed enforcing resultant force and moment equilibrium, axial stress equilibrium with internal forces and moments, interfacial strain continuity, and stress-strain relations. A solution is obtained assuming a bilinear elastic-plastic response model and is verified with the finite element package ANSYS (1993). The use of a power law elastic-plastic response model results in stress discontinuity in both layers with sufficiently large thermal loads. A new power law purely plastic response model was proposed that results in a continuous residual stress distribution and is verified with ANSYS (1993). The details of this work can be found in Tierney (1995).

Contributed by the Electrical and Electronic Packaging Division for publication in the JOURNAL OF ELECTRONIC PACKAGING. Manuscript received by the EEPD, April 18, 1995; revision received February 10, 1997. Associate Technical Editor: I. C. Ume.

Analysis

Bimaterial Configuration. The physical configuration under consideration is a strip composed of two layers perfectly bonded along the interface, as shown in Fig. 1. The heights of layers 1 and 2 are h_1 and h_2, respectively. The corresponding coefficients of thermal expansion are α_1 and α_2. The thickness of each strip is taken as b. Values used for b are sufficiently small in comparison to h_1 and h_2 so that plane stress assumptions are valid (Ugural and Fenster, 1987). Therefore, the through-thickness stresses are assumed to be zero, and the in-plane stress σ_{xx} is constant through the thickness. A general tool for design purposes is sought in this investigation, where the through height uniaxial stresses in the layers are calculated. End effects are not considered here, so the results are strictly valid only away from the free edges. The length of each layer is taken sufficiently large so that end effects are absent at $x = 0$.

Previous work has been done for this problem with a single temperature change (ΔT). This investigation is an extension where a general piecewise constant temperature versus time profile is used, allowing for multiple thermal loading and unloading as shown in Fig. 2. A solution is found for the uniaxial stress distribution at any time in a given profile. The model does assume constant material properties over the temperature range considered. A more refined solution would allow material properties to vary with each temperature step.

Bilinear Response Model. A bilinear stress-strain curve is considered as the first material response model. Isotropic hardening in assumed (Chen and Zhang, 1991). Figure 3 represents the response due to a general multiple loading scenario.

During initial loading, the slope is E (elastic modulus) until the yield stress σ_y is reached. The corresponding strain at this point is ϵ_y, the yield strain. After this point the material deforms plastically with a slope E_T (tangent modulus). For all examples done in this investigation, the values for the tangent modulus are much smaller than those used for the elastic modulus. This is done to approximate elastic, perfectly plastic materials. However, the formulation remains valid for materials that experience a greater degree of hardening.

If a material is stressed beyond the yield point, residual plastic deformation will be present upon unloading. The total mechani-

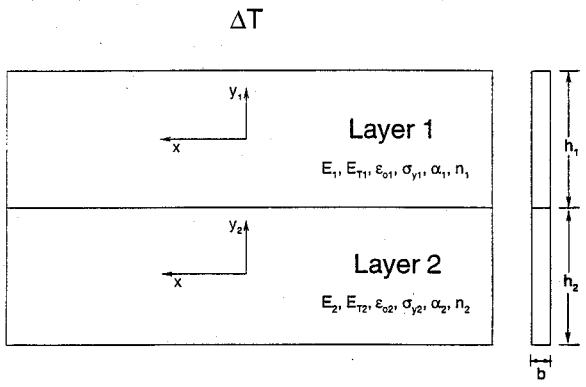

Fig. 1 Bimaterial configuration

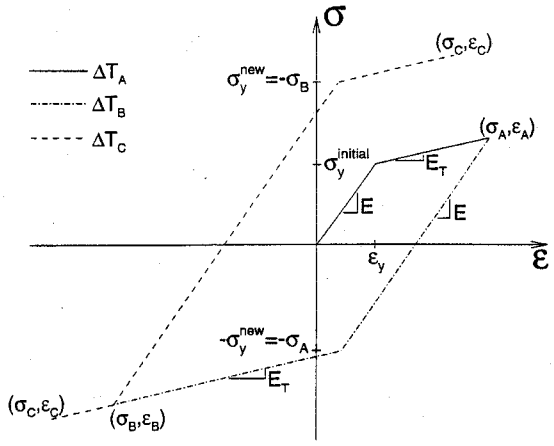

Fig. 3 Stress-strain response of multiply loaded bilinear material

cal strain ϵ is composed of an elastic strain ϵ^e and a plastic strain ϵ^p.

Expressions relating the stress and total mechanical uniaxial strain under the initial load (solid line) can be obtained by examination of Fig. 3. In the elastic region, the stress is related to the strain by Hooke's Law.

$$\sigma = E\epsilon \quad \text{for} \quad |\epsilon| \leq \epsilon_y \tag{1}$$

If the material has been stressed beyond the yield level, the stress and strain are related by

$$\sigma = \text{sign}\,(\epsilon)\,\frac{E - E_T}{E}\,\sigma_y + E_T\epsilon \quad \text{for} \quad |\epsilon| > \epsilon_y. \tag{2}$$

Equations pertaining to the stress-strain response now need to be developed that account for isotropic hardening. Every time the material is stressed beyond the yield level, a new yield stress is exhibited by the material. Assume that the material exceeds yield under ΔT_A. The dash-dotted line represents the response due to ΔT_B with load reversal (ΔT_B and ΔT_A having opposite signs). The yield stress is updated ($\sigma_y^{\text{new}} = |\sigma_A|$) for the second load to account for isotropic hardening. Assume that the material is reverse yielded under ΔT_B so that the yield stress is again updated ($\sigma_y^{\text{new}} = |\sigma_B|$). The response under a third thermal load ΔT_C is now considered. This must be general enough to allow for continued reverse yielding of the material, or reversal of the direction of stress, depending on the value of ΔT_C with respect to ΔT_B. The stress-strain value is required to lie somewhere along the dashed line in the figure and can be described as

$$\sigma_C = \sigma_B + E(\epsilon_C - \epsilon_B) \quad \text{for} \quad |\sigma_C| \leq \sigma_y^{\text{new}}$$

$$\sigma_C = \sigma_y^{\text{new}} + E_T\left[\epsilon_C - \epsilon_B - \frac{1}{E}(\sigma_y^{\text{new}} - \sigma_B)\right] \tag{3}$$

$$\text{for} \quad \sigma_C > \sigma_y^{\text{new}} \tag{4}$$

$$\sigma_C = -\sigma_y^{\text{new}} + E_T\left[\epsilon_C - \epsilon_B - \frac{1}{E}(-\sigma_y^{\text{new}} - \sigma_B)\right]$$

$$\text{for} \quad \sigma_C < -\sigma_y^{\text{new}}. \tag{5}$$

Power Law Response Model. An alternative to the bilinear model is a smooth power law stress-strain response model. The isotropic hardening model (Stoltz and Pelloux, 1977) is generalized to account for multiple loadings. Two types of responses are considered for the multiple load case: elastic-plastic response and purely plastic response.

The stress-strain response for a material exhibiting power law behavior is depicted in Fig. 4. Two different types of materials are considered, one is brittle and the other ductile.

For this investigation the power law behavior is based on the Ramberg-Osgood (Ramberg and Osgood, 1943) formulation, rewritten as

$$\epsilon = \frac{\sigma}{E} + \epsilon_o\left(\frac{\sigma}{\sigma_y}\right)^n, \tag{6}$$

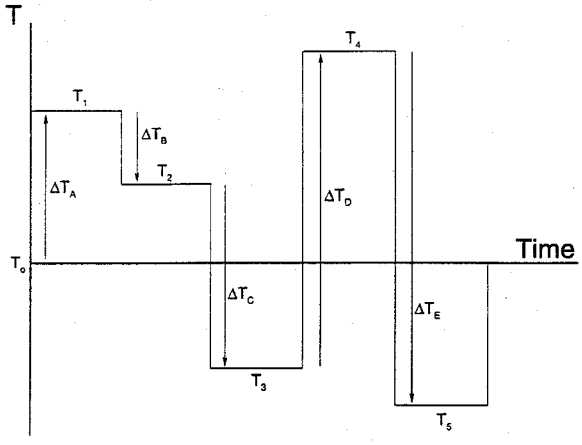

Fig. 2 General temperature profile

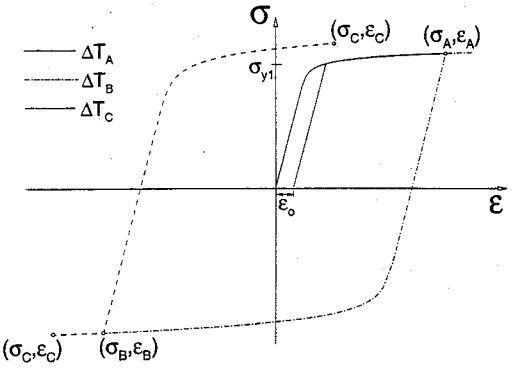

Fig. 4 Stress-strain response of multiply loaded power law material

where E is the elastic modulus, ϵ_o is the offset strain, σ_y is associated with the yield point, and n is a parameter used to fit curves through experimental stress-strain values. As is typically done for a wide variety of metals, a value of 0.002 is used for the offset strain. The value of n corresponds to the degree of plasticity that the material experiences. A value of 25 is used for all materials considered in this investigation in order to approximate elastic, perfectly plastic behavior.

During the initial loading of the material, Eq. (6) is used to relate the stress and strain. This relation is valid as long as load reversal does not occur after the yield stress has been exceeded. Assuming that the material will return along the original path to zero strain at zero load before yield, the material is taken to exhibit elastic-plastic behavior. Figure 4 shows the response under a general temperature profile. Assume that the material is yielded under ΔT_A (solid line) and reverse yielded under ΔT_B (dash-dotted line). The material response under a third temperature load ΔT_C is now sought. If ΔT_C causes strain in the same direction as under ΔT_B, the stress-strain relationship is

$$\epsilon_C = \epsilon_A + \left[\frac{\sigma_C - \sigma_A}{E} + \epsilon_o\left(\frac{\sigma_C - \sigma_A}{2|\sigma_A|}\right)^n\right], \qquad (7)$$

whereby the stress-strain response continues along the same line. If there is reversal in the direction of loading, the point (σ_B, ϵ_B) is taken as the starting point of the new curve.

$$\epsilon_C = \epsilon_B + \left[\frac{\sigma_C - \sigma_B}{E} + \epsilon_o\left(\frac{\sigma_C - \sigma_B}{2|\sigma_B|}\right)^n\right]. \qquad (8)$$

The same approach is followed for subsequent loadings. The factors $2|\sigma_A|$ and $2|\sigma_B|$ of Eqs. (7) and (8) are used in the denominator of the nonlinear component to account for isotropic hardening. This is the same approach taken in the bilinear case, although not shown explicitly in those equations. This accounts for the yield stress being updated every time the yield level is exceeded.

Another model of material response was investigated wherein all deformations are taken to be purely plastic. In this case, it is still assumed that the stress-strain curve follows a power law. During the initial loading a so-called yield stress is still used to describe the response, as in Eq. (6). However, this yield stress is not to be interpreted as the point at which plastic strains commence since the entire response is regarded as being plastic. The relations describing this response are similar to those given in Eqs. (7) and (8). The main difference is that a check is no longer required to determine if "yield" has occurred in the current load. Every time that a new stress is reached that exceeds the previous maximum stress, the so-called yield stress is updated in the equation. Figure 4 can be used to describe the response of this purely plastic model. To begin with, a maximum stress $\sigma^{\max}$ is defined as the yield stress given in the Ramberg-Osgood parameters. During the initial temperature change ΔT_A, the stress and strain are related by Eq. (6) until there is load reversal. After completion of the initial load, a check is required to see if $\sigma^{\max}$ has been exceeded by $|\sigma_A|$. If it has, then $\sigma^{\max}$ is updated to equal $|\sigma_A|$. This approach is used for all subsequent loadings.

A third thermal load ΔT_C is now considered. If this continues the load in the same direction as the previous load

$$\epsilon_C = \epsilon_A + \left[\frac{\sigma_C - \sigma_A}{E} + \epsilon_o\left(\frac{\sigma_C - \sigma_A}{|\sigma_A| + \sigma^{\max}}\right)^n\right]. \qquad (9)$$

If there is a load direction reversal from the previous load

$$\epsilon_C = \epsilon_B + \left[\frac{\sigma_C - \sigma_B}{E} + \epsilon_o\left(\frac{\sigma_C - \sigma_B}{|\sigma_B| + \sigma^{\max}}\right)^n\right]. \qquad (10)$$

If loadings are limited to occur where the stress-strain response is nearly linear, then the elastic-plastic model and the purely plastic model will yield nearly identical results. Also, if the initial load exceeds the yield stress and all subsequent loads are progressively larger, then the two models will yield the same results. The difference in the two models arises in loadings in the nonlinear elastic region of the elastic-plastic model. Upon unloading of the elastic-plastic model, the nonlinear curve is followed back to zero load. However, in the purely plastic model the unloading curve does not follow the loading curve. It will start unloading in a near linear fashion.

Governing Equations. The bimaterial strips considered in this investigation consist of two materials with different coefficients of thermal expansion. The strips are the same length and assumed perfectly bonded at the interface. When the bimaterial strip is subjected to a uniform temperature change, the layer with the larger coefficient of thermal expansion will undergo a larger thermal expansion (or contraction), thus inducing axial forces and bending moments in order to maintain continuity along the bond. These forces and bending moments will induce uniaxial stress in the strips. The deformed configuration is shown in Fig. 5. The stress distribution shown is for a bilinear response model under an initial thermal load.

In order for the strip to remain in static equilibrium throughout the thermal loading cycle, the resultant force and moment across the composite cross section must vanish, i.e.,

$$P_1 + P_2 = 0 \qquad (11)$$

$$M_1 + M_2 - \frac{P_1 h_1}{2} + \frac{P_2 h_2}{2} = 0. \qquad (12)$$

The fact that resultant force/moment are required to be zero instead of the actual stress introduces the approximation that avoids the consideration of edge effects. Imposition of the zero-stress condition requires a much more involved analysis. A state of plane stress is assumed and only uniaxial stresses are considered. The fact that the through height normal stress is neglected is consistent with bar and beam theory. The uniaxial stress distribution in each layer must be statically equivalent to the internal forces and bending moments.

$$\int_{-h_1/2}^{h_1/2} \sigma_1 b dy_1 = P_1 \qquad (13)$$

$$\int_{-h_2/2}^{h_2/2} \sigma_2 b dy_2 = P_2 \qquad (14)$$

$$\int_{-h_1/2}^{h_1/2} \sigma_1 y_1 b dy_1 = -M_1 \qquad (15)$$

$$\int_{-h_2/2}^{h_2/2} \sigma_2 y_2 b dy_2 = -M_2 \qquad (16)$$

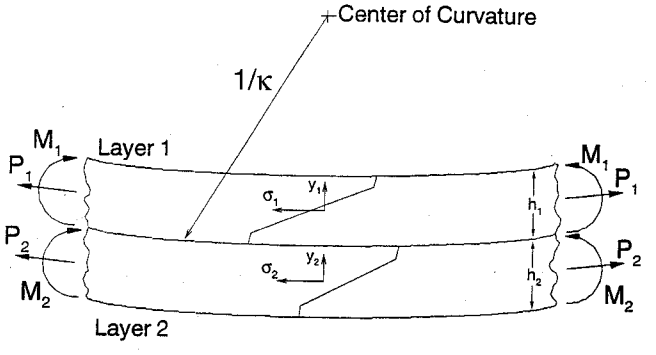

Fig. 5 Deformed configuration due to a thermal load

In these equations, σ_i refers to the internal axial stress (σ_{xx}) in the ith layer and y_i is the coordinate used to measure the distance from the centroidal axis in the ith layer.

During a multiple thermal load analysis every point along the y-direction in each layer may follow a different stress-strain path, depending on the extent of yielding and reverse yielding. Thus the solution is highly path dependent. In this case it is not possible to write closed form equations for the stress and strain for distinct regions of each layer. Instead, each layer is discretized into m discrete stress sites and all integrations are carried out numerically using the trapezoidal rule. Equations (14)–(16) are treated similarly. In the power law response approach Simpson's rule is used to numerically integrate Eqs. (13)–(16) to more accurately account for the nonlinear behavior of the material. All example problems use $m = 101$ stress sites in each layer. Fewer sites are required for brittle materials because the stress distribution is nearly linear.

When the bimaterial configuration deforms due to a thermal load, both mechanical strains ϵ (tension and bending) and thermal strains ϵ^T are developed. The total strain ϵ^{tot} is then the sum of both mechanical and thermal strains.

$$\epsilon^{\text{tot}} = \epsilon + \epsilon^T \tag{17}$$

The mechanical strain is decomposed into a uniform axial strain $\bar{\epsilon}$ which is independent of y and a bending component related to the curvature κ according to

$$\epsilon = \bar{\epsilon} - \kappa y. \tag{18}$$

Note that κ is equal to the inverse of the radius of curvature ρ. The value for the curvature is taken to be the same for both layers. This will not result in significant error because the resulting values for the radius of curvature are much larger than the heights of the individual layers. The thermal strain can be written as

$$\epsilon^T = \alpha \Delta T_k, \tag{19}$$

where α is the coefficient of thermal expansion and ΔT_k is the kth thermal load.

The assumption has been made that a perfect bond exists between the two layers. This condition that reflects continuity of total axial strain along the interface is

$$\epsilon^{\text{tot}}_{1,m} = \epsilon^{\text{tot}}_{2,1}. \tag{20}$$

Upon introducing expressions for the total axial strain along the interface this becomes

$$\bar{\epsilon}_1 + \frac{h_1}{2}\kappa + \alpha_1 \Delta T_k = \bar{\epsilon}_2 - \frac{h_2}{2}\kappa + \alpha_2 \Delta T_k. \tag{21}$$

Each of the m stress sites in each layer is required to follow the stress-strain response of Eqs. (3)–(5) for bilinear response materials, Eqs. (6)–(8) for elastic-plastic power law response materials, or Eqs. (6), (9) and (10) for purely plastic power law response materials.

Together, Eqs. (11)–(16), (21), and the $2m$ equations of the form shown in Eqs. (3)–(5), (6)–(8), or (6), (9) and (10) (depending on the material response model chosen) define a system of $7 + 2m$ nonlinear algebraic equations in $7 + 2m$ unknowns. The unknowns are then P_1, P_2, M_1, M_2, $\bar{\epsilon}_1$, $\bar{\epsilon}_2$, κ, and stresses at m stress sites in layers 1 and 2 – $\sigma_{1,j}$, $\sigma_{2,j}$ ($j = 1, 2, \ldots m$). The iterative Newton method described in Burden and Faires (1989) was used to solve this system of equations. The terms in the associated Jacobian matrix were all established analytically in order to take advantage of the convergence characteristics of the Newton scheme. See the Appendix for further details concerning implementation of the solution strategy for the system of equations.

Electronic Materials. As the problem under consideration is concerned with microelectronic packaging, the materials chosen to illustrate the solution are common to this industry. The properties used are the same as found in Eischen and Reagan (1993) and Cifuentes (1991). Several of the examples considered in those works are extended to account for multiple loadings and unloadings. Table 1 shows the properties used in this analysis. The values listed are for both bilinear and power law stress-strain response models. They include the elastic modulus E and tangent modulus E_T. Note that in all cases the tangent modulus is a small fraction the elastic modulus, in order to approximate elastic, perfectly plastic behavior. However, the tangent modulus values are nonzero so that the formulation is applicable to materials that exhibit a great degree of strain hardening. Values for the yield stress σ_y are also given, and are used in both bilinear and power law formulas. Note that σ_y simply denotes a curve fitting parameter for the power law purely plastic scenario, and not the yield stress as is common in elastic-plastic analyses. The coefficients of thermal expansion α are also included, as are values for the offset strain ϵ_o and power law exponent n. The values used for the offset strain and power law exponent are the same for all materials. The properties given indicate falsely that silicon is quite ductile. These properties are fictionalized for the sake of illustrating the model.

Results

In the following examples, the predicted uniaxial stress distribution is plotted along with results obtained from the finite element package ANSYS (1993). A plane of symmetry exists through the mid-span of the configuration (along the y-axis) so symmetry boundary conditions are used on one side of the ANSYS model. Twenty elements were used through the height of each layer, and five to twelve elements were used along the length of the strip. The model consists of four-node quadrilateral plane stress elements. ANSYS allows the material characteristics to be defined for either bilinear or multilinear stress-strain curves. An option allowing for isotropic hardening was also used. In the analytical solution, $m = 101$ stress sites are through the height of each layer.

Example 1 concerns a silicon/aluminum strip with both materials modeled as bilinear. The initial thermal load consists of cooling from an annealing temperature of 450°C to room temperature, 25°C ($\Delta T_1 = -425$°C). The second thermal load is a heating of the device from room temperature to a standard operating temperature of 150°C ($\Delta T_2 = +125$°C). This is a realistic temperature profile for a device constructed by chemical vapor deposition (Sze, 1988). The residual uniaxial stress distribution under both loads is shown in Fig. 6. There is considerable residual stress in the configuration as it cools from the annealing temperature to room temperature. A large portion of the silicon layer is shown to have exceeded the yield stress, either in tension at the top of the layer or in compression at the bottom of the layer. Yielding in tension is found in the aluminum layer. Note that the stress values listed in the figure at the layer boundaries are from the analytical solution. There is very good agreement between the analytical and ANSYS solutions under both loads in the silicon layer. The solution is not quite as accurate in the aluminum layer, but the shape of the stress distribution and extreme values match up well. The model used here indicates that the manufacturing process will have a large

Table 1 Material properties used in examples

	E 10^{10} Pa	E_T Pa	σ_y 10^8 Pa	α 10^{-6}/°C	ϵ_o	n
Silicon(Si)	20.0	2.0×10^2	2.6201	2.5	0.002	25
Molybdenum(Mo)	32.5	1.0756×10^9	5.1713	4.9	0.002	25
Aluminum(Al)	7.0	2.0×10^8	1.54	23.0	0.002	25
Copper(Cu)	13.24	7.309×10^8	0.6895	16.1	0.002	25

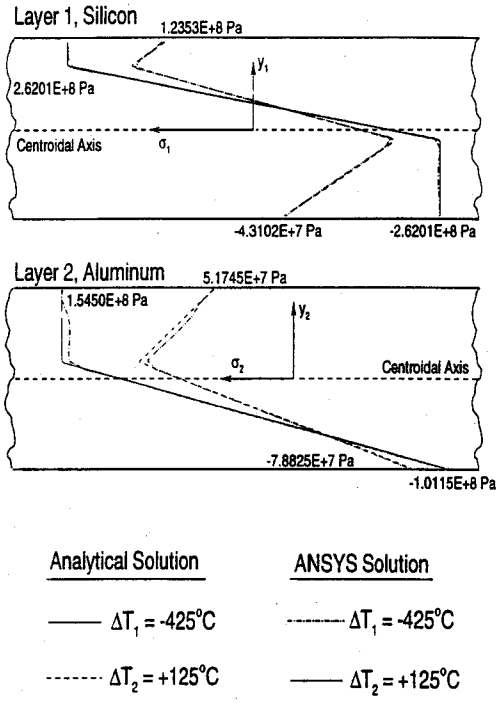

Fig. 6 Stress distributions for silicon/aluminum strip, Example 1

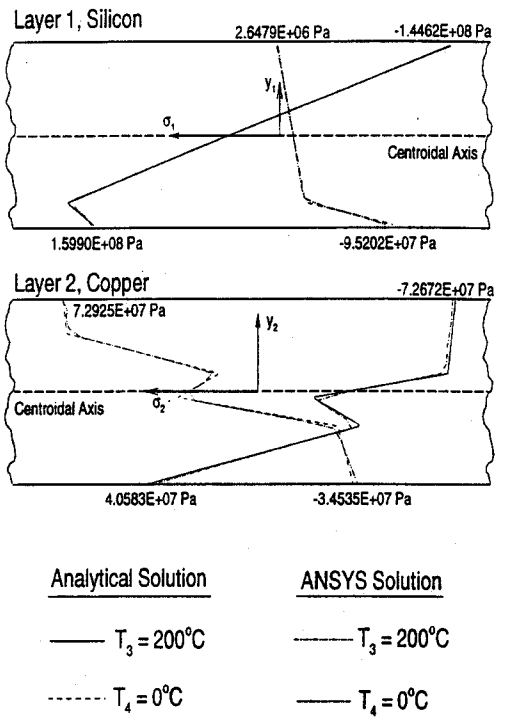

Fig. 7 Stress distributions for silicon/copper strip, (ΔT_3 and ΔT_4), Example 2

impact on the performance of microelectronics during standard operation. When cycling between room temperature and typical circuit operating temperature, the internal stresses will vary between the two temperature dependent distributions shown in the figure. The portions of the layers that are stressed beyond the yield point will be associated with large amounts of plastic strain, due to the relatively small values used for the tangent modulus in both materials. This can lead to warpage or fracture of the component.

The second example concerns a silicon/copper strip subjected to a temperature profile consisting of four thermal loads ($\Delta T_1 = +300°C$, $\Delta T_2 = -400°C$, $\Delta T_3 = +300°C$, and $\Delta T_4 = -200°C$). This is a contrived example chosen to show the utility of solution. A bilinear response model is assumed for both layers. The stress distribution under ΔT_3 and ΔT_4 is given in Fig. 7. Under ΔT_1, the silicon yields in tension at the bottom of the layer and the copper yields in compression at the top of the layer. The silicon layer is stressed elastically under subsequent thermal loading. The copper layer experiences reverse yielding with each load reversal. Continued reverse yielding results in a multilinear stress distribution. The ANSYS solution loses accuracy upon multiple loads due to the coarseness of the mesh used. ΔT_4 brings the strip back to the original temperature. Although the strip has undergone no net temperature change, there is considerable residual stress present in both layers.

Example 3 consists of a molybdenum/aluminum strip that is heated 1000°C and then cooled to the original temperature. The bilinear response model and both the elastic-plastic and purely plastic power law response models are used, and the results shown in Fig. 8. Under the initial ΔT_1 load, the bilinear model and power law model give similar stress distributions. ANSYS was able to verify the results of the bilinear model and it was expected that the power law model should give similar results upon multiple loads. However, the original elastic-plastic model used for the power law approach varied greatly from the bilinear model, as can be seen in the figure. The elastic-plastic unloading model leads to stress discontinuity in both layers. This led to the formulation of the purely plastic unloading model. This new model was shown to follow the stress curve of the bilinear model more closely.

A silicon/copper strip is considered in example 4. The initial thermal load consists of heating the strip by 400°C, and the strip is cooled to the original temperature under the second thermal load. The two power law response models are compared

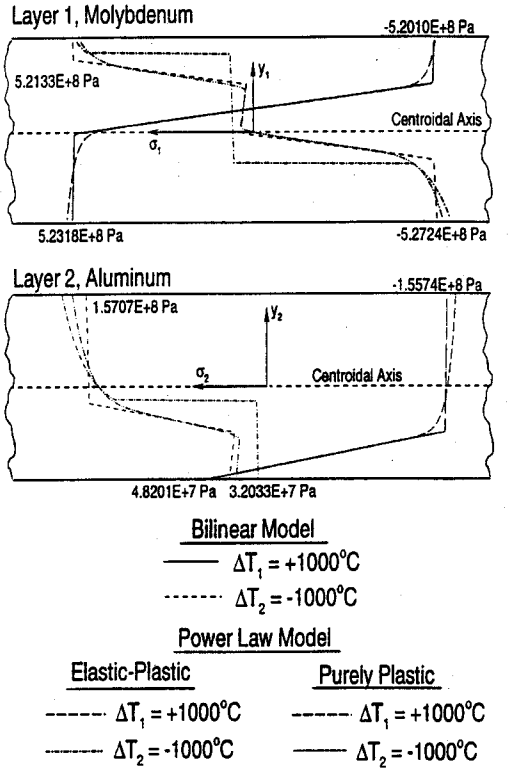

Fig. 8 Stress distributions using different models, molybdenum/aluminum strip, Example 3

with ANSYS. The results are given in Fig. 9. ΔT_1 does not cause yielding in the silicon layer, and upon unloading the stresses return to near-zero values using the elastic-plastic unloading model. However, the purely plastic unloading model and ANSYS show a very different residual stress distribution. The top of the copper layer is stressed beyond σ_y under ΔT_1. This leads to a stress discontinuity under ΔT_2 using the elastic-plastic unloading model. The resulting stress distribution using the purely plastic unloading model is verified from the ANSYS results. The ANSYS results and the purely plastic model differ at nonlinear regions of the stress distribution because ANSYS assumes linear unloading up to the point of reverse yielding.

The final example concerns a silicon/aluminum strip. The strip is subjected to the same temperature loading as in chapter 1, and a purely plastic power law model is used for both materials and compared with ANSYS. There is excellent agreement between the two solutions as shown in Fig. 10. The bottom portion of the silicon layer and the top portion of the aluminum layer are stressed beyond "yield" under ΔT_1. The stress in both layers are reduced due to ΔT_2.

Conclusions

The residual stress distribution in a bimaterial configuration induced by multiple piecewise constant temperature excursions has been investigated. Both bilinear and power law models were used, and reverse yielding was allowed to occur according to an isotropic hardening law. Examples with realistic temperature versus time profiles predict significant residual stress distributions present in microelectronics during manufacture. The bilinear response model and purely plastic power law response model were verified with the finite element package ANSYS using materials common to the microelectronic packaging industry. The use of an elastic-plastic power law stress-strain response model leads to stress discontinuity under multiple temperature loads with load reversal.

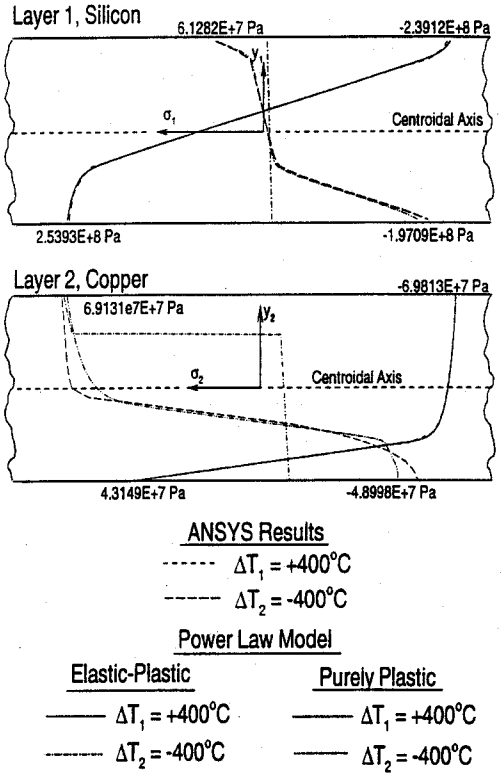

Fig. 9 Stress distributions for silicon/copper strip, Example 4

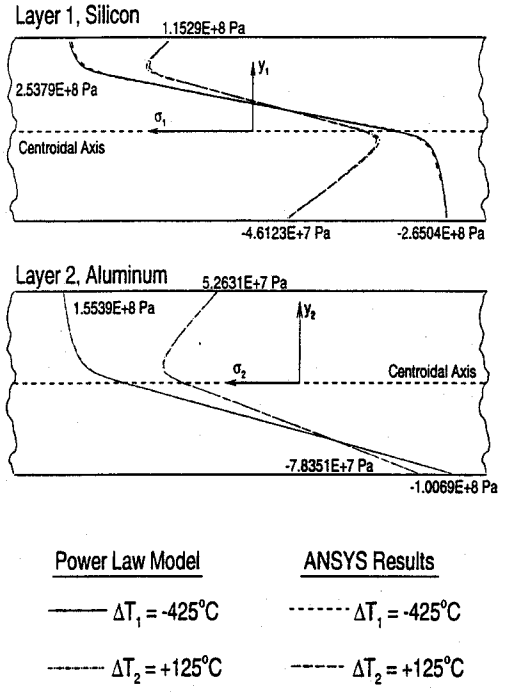

Fig. 10 Stress distributions for silicon/aluminum strip, Example 5

References

ANSYS User's Manual for Revision 5.0, 1993, Swanson Analysis Systems, Inc.

Burden, R. L., and Faires, J. D., 1989, *Numerical Analysis,* PWS-Kent Publishing Co., Boston, MA, pp. 536–539.

Chen, W. F., and Zhang, H., 1991, *Structural Plasticity: Theory, Problems, and CAE software,* Springer-Verlag Inc., pp. 7–14.

Cifuentes, A. O., 1991, "Elastoplastic Analysis of Bimaterial Beams Subjected to Thermal Loads," ASME JOURNAL OF ELECTRONIC PACKAGING, Vol. 113, pp. 355–358.

Eischen, J. W., and Reagan, S. W., 1993, "Elastic Plastic Analysis of Bimaterial Beams With Strain Hardening," *Proceedings of the 10th Biennial Conference on Reliability, Stress Analysis, and Failure Prevention,* DE-Volume 55, The American Society of Mechanical Engineers, pp. 289–296.

Ramberg, W., and Osgood, W. R., 1943, "Description of Stress-Strain Curves by Three Parameters," Technical Note No. 902, National Advisory Committee for Aeronautics (NACA).

Stoltz, R. E., and Pelloux, R. M., 1977, "The Bauschinger Effect, Monotonic and Cyclic Hardening in Precipitation-Strengthened Aluminum Alloys," *Work Hardening in Tension and Fatigue* (Proceedings), Mechanical Metallurgy Committee, pp. 224–239.

Suhir, E., 1988, "An Approximate Analysis of Stresses in Multilayered Elastic Thin Films," ASME *Journal of Applied Mechanics,* Vol. 55, pp. 143–148.

Sze, S. M., 1988, *VLSI Technology,* McGraw-Hill Book Co., NY, p. 385.

Tierney, J. W., 1995, "Residual Stress Analysis of Bimaterial Strips Under Multiple Thermal Loading," M.S. thesis, North Carolina State University at Raleigh, NC.

Timoshenko, S., 1925, "Analysis of Bi-Metal Thermostats," *Journal of the Optical Society of America,* Vol. 11, pp. 233–255.

Ugural, A. C., and Fenster, S. K., 1987, *Advanced Strength and Applied Elasticity,* Elsevier Science Publishing Co. Inc., NY, pp. 69–71.

APPENDIX

The first step in implementing the Newton Raphson solution technique is to rearrange the governing equations so that the right hand side is equal to zero. The governing equations for the bilinear response will be shown in detail.

$$f_1 = P_1 + P_2 = 0 \tag{22}$$

$$f_2 = M_1 + M_2 - \frac{P_1 h_1}{2} + \frac{P_2 h_2}{2} = 0 \tag{23}$$

$$f_3 = \frac{bh_1}{2m}\left[\sigma_{1,1} + 2\sum_{j=2}^{m-1}\sigma_{1,j} + \sigma_{1,m}\right] - P_1 = 0 \tag{24}$$

$$f_4 = \frac{bh_2}{2m}\left[\sigma_{2,1} + 2\sum_{j=2}^{m-1}\sigma_{2,j} + \sigma_{2,m}\right] - P_2 = 0 \quad (25)$$

$$f_5 = \frac{bh_1}{2m}\left[\sigma_{1,1}y_{1,1} + 2\sum_{j=2}^{m-1}\sigma_{1,j}y_{1,j} + \sigma_{1,m}y_{1,m}\right] + M_1 = 0 \quad (26)$$

$$f_6 = \frac{bh_2}{2m}\left[\sigma_{2,1}y_{2,1} + 2\sum_{j=2}^{m-1}\sigma_{2,j}y_{2,j} + \sigma_{2,m}y_{2,m}\right] + M_2 = 0 \quad (27)$$

$$f_7 = \bar{\epsilon}_1 + \frac{h_1}{2}\kappa + \alpha_1\Delta T_k - \bar{\epsilon}_2 + \frac{h_2}{2}\kappa - \alpha_2\Delta T_k = 0 \quad (28)$$

$$f_{2m} = \sigma_{i,j}^k - \sigma_{i,j}^{k-1} - E(\epsilon_{i,j}^k - \epsilon_{i,j}^{k-1}) = 0 \text{ for } |\sigma_{i,j}^k| \le \sigma_y^{\text{new}} \quad (29)$$

$$= \sigma_{i,j}^k - \sigma_y^{\text{new}} - E_T\left[\epsilon_{i,j}^k - \epsilon_{i,j}^{k-1} - \frac{1}{E}(\sigma_y^{\text{new}} - \sigma_{i,j}^{k-1})\right] = 0$$

$$\text{for} \quad \sigma_{i,j}^k > \sigma_y^{\text{new}} \quad (30)$$

$$= \sigma_{i,j}^k + \sigma_y^{\text{new}} - E_T\left[\epsilon_{i,j}^k - \epsilon_{i,j}^{k-1} - \frac{1}{E}(-\sigma_y^{\text{new}} - \sigma_{i,j}^{k-1})\right] = 0$$

$$\text{for} \quad \sigma_{i,j}^k < -\sigma_y^{\text{new}} \quad (31)$$

where the index i refers to the layer number. Define $\mathbf{F}$ to be a column vector of these equations

$$\mathbf{F} = [f_1, f_2, f_3, \ldots, f_{7+2m}]^T \quad (32)$$

Let x^k be a vector of the unknowns

$$x^k = [P_1, P_2, M_1, M_2, \bar{\epsilon}_1, \bar{\epsilon}_2, \kappa, \sigma_{1,1}, \sigma_{1,2}, \ldots, \sigma_{1,m}, \sigma_{2,1}, \sigma_{2,2}, \ldots, \sigma_{2,m}]^T \quad (33)$$

where $x_1 = P_1$, $x_2 = P_2$, and so on. The Jacobian matrix for the system is calculated according to

$$J_{ij} = \frac{\partial f_i}{\partial x_j}. \quad (34)$$

Several terms of the Jacobian are presented here as examples

$$J_{11} = \frac{\partial f_1}{\partial P_1} = 1 \quad (35)$$

$$J_{3,8} = \frac{\partial f_3}{\partial \sigma_{1,1}} = \frac{bh_1}{2m} \quad (36)$$

$$J_{7,7} = \frac{\partial f_7}{\partial \kappa} = \frac{1}{2}(h_1 + h_2) \quad (37)$$

$$J_{8,5} = \frac{\partial f_8}{\partial \bar{\epsilon}_1} = -E_T \quad \text{for} \quad |\sigma_{i,j}^k| > \sigma_y^{\text{new}}. \quad (38)$$

The $(7 + 2m)$ by $(7 + 2m)$ linear system of algebraic equations

$$J_{ij}\Delta x_j = -F_i \quad (39)$$

must be solved for Δx_j, which is used to update the solution for the current iteration k

$$x_i^{k+1} = x_i^k + \Delta x_i. \quad (40)$$

This process is repeated until the change in Δx is sufficiently small (convergence).